

Analysis and Modeling of Low Pressure CVD of Silicon Nitride from a Silane-Ammonia Mixture

I. Experimental Study and Determination of a Gaseous Phase Mechanism

Khalid Yacoubi,^a Catherine Azzaro-Pantel,^{a,z} E. Scheid,^b and Jean-Pierre Couderc^a

^aLaboratoire de Génie Chimique UMR CNRS 5503-ENSIGC INPT/UPS, 31078 Toulouse Cedex 04, France

^bCNRS, Laboratoire d'Analyse et d'Architecture des Systèmes, 31077 Toulouse Cedex, France

This paper, Part I of two, presents the results of a study combining experimental and modeling approaches of low pressure chemical vapor deposition (LPCVD) of silicon nitride from a silane-ammonia mixture. The experimental study consists in a reduced number of runs, chosen in order to identify the main features of the deposition process, *i.e.*, marked nonuniformities at the wafer edge both in thickness and in Si/N composition. It is then shown that a complex gas-phase mechanism may be responsible for the observed physicochemical phenomena. A gaseous reaction model is thus proposed for a silane-ammonia mixture under typical low pressure CVD conditions. A complete reaction scheme is first studied. A thorough quantum Rice Ramsberger Kassel (QRRK) analysis compensated for the lack of kinetic information in the gas phase and allowed the identification of kinetic constants for uni- and bimolecular reactions. Its appropriateness is examined with one-dimensional nonsteady computations. A combined analysis of these calculations and of the QRRK results shows that the reaction model could be simplified, thus leading to a reduced reaction set reproducing the essential features of the full mechanism experimentally observed, which involves six species with two silylamine intermediates SiH₃NH₂ and SiHNH₂. In Part II of this article series, this mechanism is integrated in a 2-D model of LPCVD reactors, previously developed in the laboratory (called CVD2) and adapted to this kind of deposition, taking into account hydrodynamics, mass transport, and chemical reactions.

© 1999 The Electrochemical Society. S0013-4651(98)10-087-3. All rights reserved.

Manuscript submitted October 22, 1998; revised manuscript received April 11, 1999.

Several processes are generally carried out for the production of silicon nitride films, commonly used as insulation or passivation materials within the metal oxide semiconductor (MOS) technology: plasma enhanced chemical vapor deposition (PECVD), low pressure CVD (LPCVD), and, more recently, rapid thermal processing (RTP). The different processes and gas sources are presented in Table I. The typical operating conditions, the order of magnitude of deposition rate, and the etching rate are briefly recalled. The choice of atmospheric pressure has long been replaced by low pressure (about 1 Torr); in these conditions, the diffusion of reactant species is much more rapid, thus leading to more uniform layers. The advantage of the plasma process is to use relatively low deposition temperature. Note that this technique is mainly carried out for silicon nitride films used as final passivation layers due to the final film features (*i.e.*, high deposition rates and etching rates). This investigation is focused on the production of intermediate insulating layers, and, in these conditions, the plasma process was thus discarded. Although mentioned in Table I as an emerging process, the RTCVD technique is, till now, restricted to laboratory scale. Consequently, only the LPCVD process is considered in this study, using a conventional tubular horizontal hot-wall reactor. A major advantage of such reactors is their high productivity; a hundred wafers, more can be treated simultaneously. A stringent specification for microelectronics practitioners concerns the production of uniform layers. This condition is required both for deposition rate and layer composition, and is necessary for across-wafer and across-load properties. This constraint satisfaction is generally a key point of such processes.

Silicon nitride films are generally produced by using a mixture of either dichloro-, tetrachloride- or mono- silane, and ammonia in the 700-1000°C temperature range (see Table II). To date, most investigations reported in the literature deal with silicon nitride deposition from SiCl₄-NH₃.^{1,5} Note that the disilane-ammonia mixture is only used at the laboratory level. It is generally admitted that a dichlorosilane-ammonia mixture leads to across-wafer and across-load uniformity. Only the results of Roenigk and Jensen⁵ mention important radial and longitudinal nonuniformities for a NH₃/SiH₂Cl₂ ratio ranging between 3 and 20. Such films are generally affected by the presence of holes in the layer when carried out on SiO₂, which may be attributed to the presence of not very dense adsorption sites on this surface. Besides, in these conditions, it is difficult to achieve thicknesses greater than 2000 Å, due to high stress in the film.

Except for the work of Roenigk and Jensen, it is generally reported in most studies that silicon nitride deposition is insensitive to operating conditions: uniform layers are generally obtained and the deposited silicon nitride is stoichiometric. Some works mention that NH₄Cl is likely to be formed in the preheating zone of the reactor, which may be detrimental to the pumping system. These features are also valid for depositions carried out from a tetrachlorosilane-ammonia mixture.

Very few studies have been devoted to the silane-ammonia case, although the following processing difficulties are generally encountered

1. Growth rate decreases markedly relative to pure polysilicon deposition.

2. A significant radial nonuniformity is reported, both in deposition rate and film composition (Si/N molar ratio), creating the so-called bull's eye effect. To prevent this phenomenon, engineers usu-

* Electrochemical Society Active Member.

^z E-mail: catherine.azzaro@ensigct.fr

Table I. Silicon nitride processes.

| Si ₃ N ₄ process | Temperature range (°C) | Pressure range | Deposition rate (Å/min) | Etching rate HF 50% (Å/min) | References |
|--|------------------------|----------------|-------------------------|-----------------------------|------------|
| CVD | 850-950 | atmospherical | 40 | 200-300 | 1 |
| LPCVD | 750-850 | 0.2-0.6 Torr | 20-50 | 50-100 | 2 |
| PECVD | 230-500 | 0.4-2 Torr | 60-1000 | 1500-3000 | 3 |
| RTCVD | 580-645 | 0.1-1 Torr | 50-150 | 300-500 | 4 |

Table II. Operating conditions for silicon nitride deposition.

| Gas source | Temperature range (°C) | Pressure (Torr) | Flow rates (sccm) | Deposition rate (Å/min) | Deposition uniformity | References |
|---|------------------------|-----------------|-------------------|-------------------------|---|------------|
| SiH ₂ Cl ₂ -NH ₃ | 700-900 | 0.35-0.95 | 25 + (50-400) | 25-100 | good (only Roenigk and Jensen ⁵ mention a nonuniformity of about 2.5-26.4 %) | 5 |
| SiCl ₄ -NH ₃ | 750-900 | 1-5 | 35 + (100-350) | 12-25 | good | 1 |
| SiH ₄ -NH ₃ | 800-1050 | 10-40 | 26 + 480 | 20-700 | >40 % | 1 |
| Si ₂ H ₆ -NH ₃ | 555-600 | 0.1-0.4 | (3-10) + 200 | 5-12 | 12-26 (%) | 2 |

ally resort to perforated quartz cages inserted in the LPCVD reactor around the stacked wafers, thus forming a shrouded zone in which the gas only enters through small holes. However, the design and maintenance of such cages are difficult and expensive. Besides, their use is prejudicial to an automated loading.

3. A longitudinal decrease in deposition rate is generally observed and strongly dependent on the NH₃/SiH₄ ratio.

Another gas source was mentioned in Table II, *i.e.*, a disilane-ammonia mixture, which has motivated a great interest for the production of silicon nitride films at low temperature (inferior to 600°C). This promising approach is still under investigation.⁴ Although this process is interesting to compete with the usual techniques, the understanding of the underlying physicochemical phenomena involves first a thorough study of the more classical process carried out from a silane-ammonia mixture. Without expounding on the gaseous chemical phenomena, it must be emphasized that the previous works about polycrystalline silicon deposition have clearly shown the major role of a radical species, *i.e.*, silylene, produced in the gas phase both from silane and disilane pyrolysis.

The purpose of this work is to combine both modeling and experimental analysis in order to elucidate the complex physicochemical phenomena involved in the deposition process from a silane-ammonia mixture. The presentation of this study is divided in two parts. Due to the lack of kinetic information available in the literature, a major part of this work has been focused on the investigation of gas phase reactions. The first part is devoted to the presentation of the experimental investigation which was necessary to analyze the nature of the physicochemical phenomena involved. A detailed presentation of the gaseous mechanism is then proposed. A QRRK (quantum Rice Ramsberger Kassel) analysis was carried out to compensate for the lack of kinetic information in the gas phase. A reduced reaction set reproducing the essential features of the full mechanism and involving six species including two silylamine intermediates SiH₃NH₂ and SiHNH₂ has been identified and presented. The second part of the article is focused on 2-D modeling of silicon nitride deposition. Experimental results of silicon nitride deposition will be compared with the predictions of the CVD2 model previously developed in our laboratory.^{6,7}

Experimental

Operating conditions.—Experiments were carried out in a conventional tubular horizontal hot-wall LPCVD reactor, in which 82 p-type <100> Si wafers were stacked vertically. The main characteris-

tics of the equipment used are presented in Table III. Four test wafers were placed at selected locations along the length of reactor (57, 62, 67, 72). The position of each wafer in the batch is numbered from the first wafer reached by the gases. Three boats were used and placed coaxially in the reactor one after another. The boats were separated by a distance of 5 cm. The first boat was placed next to the inlet door of the reactor and the test wafers were placed inside the flat temperature zone of the reactor. Experiments were performed at four temperatures: 650, 700, 750, and 800°C. Pressure was set at 0.4 Torr. As gaseous sources, pure silane and ammonia with a ratio 0.4/0.6 were used. The silane flow rate was maintained at 180 standard cubic centimeters per minute (sccm) and 270 sccm of ammonia was injected. Two load configurations were used (see Fig. 1).

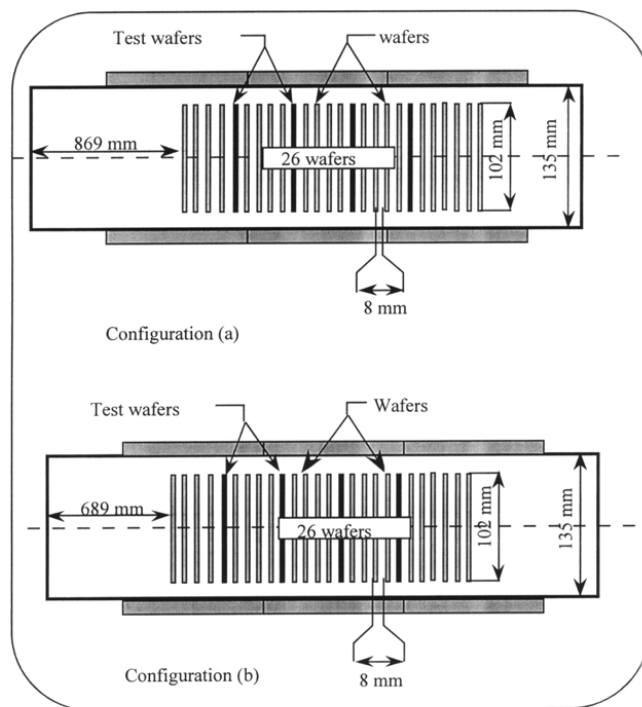
Film characterization.—The deposited films were characterized by two techniques, if necessary coupled, ellipsometry and profilometry. Thickness was measured at the center and also at the periphery of each test wafer, so as to determine the importance of the bull's eye effect, and the film composition, *i.e.*, molar ratio Si/N, was measured.

Film thickness was measured by ellipsometry at a wavelength of 405 or 803 nm. The results obtained were confirmed by plasma etching and measurements of the height of the chemically created step with TENCOR equipment.

Difficulties were encountered when using profilometry for measuring across-wafer thickness for two reasons. First, the chemical

Table III. Reactor geometry.

| Geometrical parameters | |
|---------------------------|----------|
| Tube length (m) | 1.97 |
| Tube diameter (mm) | 135 |
| Wafer diameter (mm) | 100.4 |
| Interwafer distance (mm) | 8 |
| Boat number | 3 |
| Wafer number in each boat | 28/28/26 |

**Figure 1. Reactor configurations.**

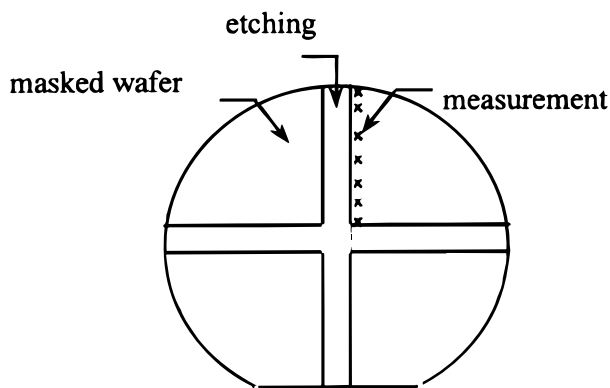


Figure 2. Wafer front view after etching.

etch between the substrate and the deposited layer must be selective, and second, the mask resistance must be efficient. The resin mask is disposed along a cross, the center of which corresponds to the wafer one, as presented in Fig. 2. Two kinds of etches can be distinguished, either wet or dry. Wet etching by fluoridric acid (HF 50%) has the advantage to be selective. But to our knowledge, no resin, either positive nor negative, can resist acid attack during a long etching time. Conversely, dry etching with SF₆ is nonselective and attacks simultaneously the deposited silicon nitride and the substrate. Thickness measurement was thus carried out with a two-stage method, as presented in Fig. 3 and 4 ($d = H_1 - H_2$).

Film composition is an essential data for a further development and validation of a simulation model of an LPCVD reactor and conditions the electrical quality of the deposited layer. The Si/N molar ratio was determined using the correlation of Dehan *et al.*⁴ In this paper, only the final expression proposed by these authors is given

$$\text{Si/N molar ratio} = x = -\frac{24n^4 - 336n^2 - 768}{7n^4 + 352n^2 - 224}$$

where n is the refractive index at 803 nm, $2 \leq n \leq 4$. The refractive index, n , was determined by coupling ellipsometry and profilometry according to the approach proposed in Fig. 4.

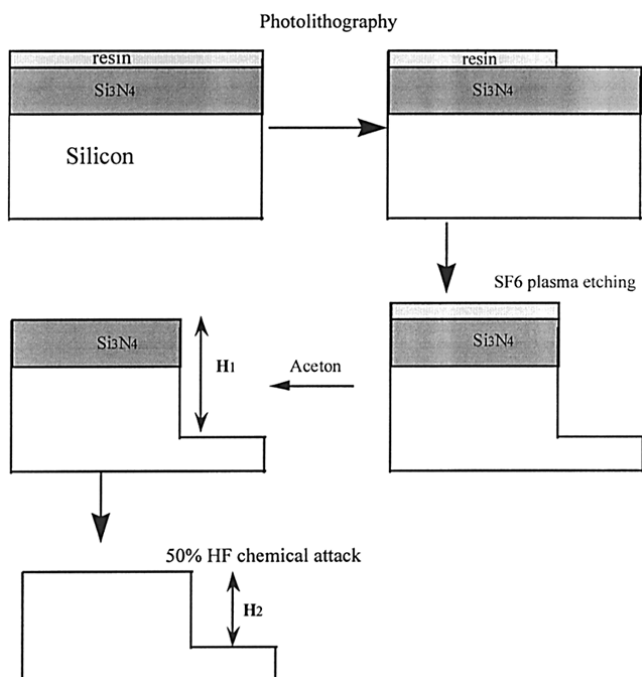


Figure 3. Principle of thickness measurement ($d = H_1 - H_2$).

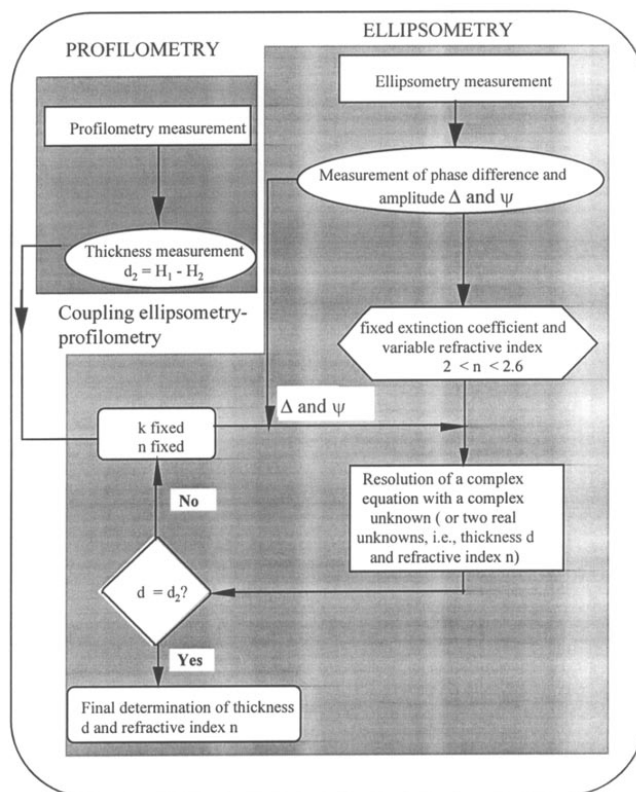


Figure 4. Coupling of the two measurement methods.

Results^c

Temperature influence.—Longitudinal evolution of silicon nitride deposition rate measured at the wafer center is presented in Fig. 5 for different temperatures. The radial evolution of the silicon nitride deposition rate at a temperature of 750°C for wafers 5 and 20 is displayed in Fig. 6. A typical profile of film composition is proposed in Fig. 7. The results obtained clearly show that

1. Ellipsometry and profilometry measurements are generally in good agreement at the wafer center but diverge at the wafer edge. Radial heterogeneities are stronger by profilometry than by ellipsometry, which may be attributed to variations in chemical composition at the wafer edge, thus reducing the value of the extinction coefficient.
2. Deposition rate stabilizes rather slowly, from the 15th wafer of the load. For the run at 650°C, a stabilization is obtained before the 10th wafer.

^c Only the most significant results are presented and analyzed in this section.

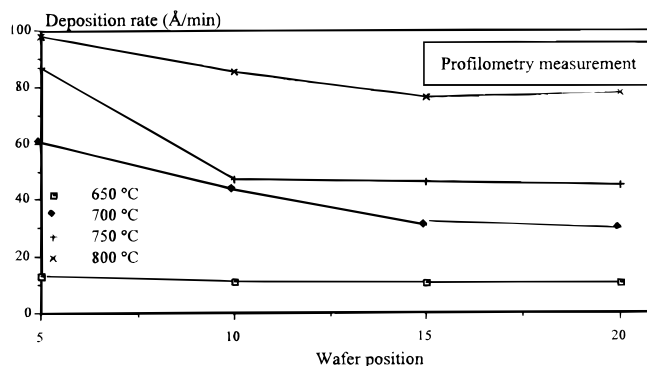


Figure 5. Longitudinal evolution of silicon nitride deposition rate for different temperatures.

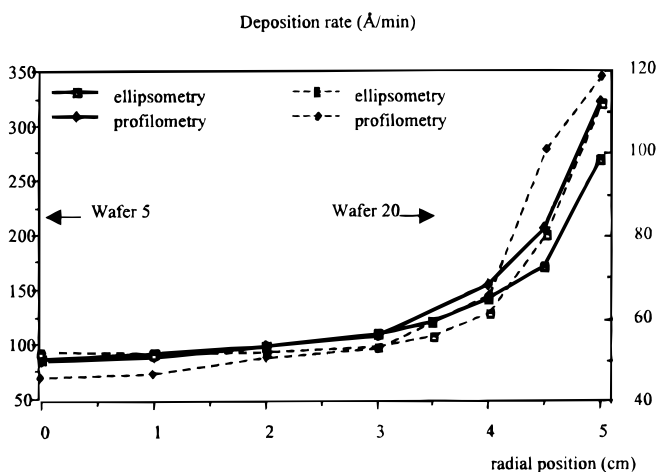


Figure 6. Radial evolution of silicon nitride deposition rate at a temperature of 750°C for wafers 5 and 20.

3. The ratio between the deposition rate measured at the wafer edge and at the center shows high radial nonuniformities: the deposition rate at the wafer periphery is approximately three times greater than that measured in the center. These nonuniformities are less marked in the exit zone of the reactor.

4. The increase in temperature of about 50°C results in an increase in deposition rate (it is doubled even tripled along the load). Radial nonuniformities increase in the same proportion.

5. The Si/N molar ratio decreases along the load (*i.e.*, silicon depletion) but increases across a wafer. This ratio increases with temperature. Note that these variations are relatively low and the Si/N molar ratio is in the range 0.74-0.81 at the wafer center and reaches 0.95 at the edge. In a stoichiometric nitride, $x = 0.75$.

Load position influence.—The influence of this parameter was tested at a temperature of 750°C. From the results obtained, it can be said that

1. An increase of the entrance zone length involves an increase in deposition rate (Fig. 8). This effect is, above all, sensitive for about the 10 first wafers of the load. But the influence of the entrance zone is not so marked as in the case of *in situ* phosphorus doped polycrystalline silicon from a silane-phosphine mixture.^{8,9}

2. Longitudinal evolution of deposition rates decreases with a different slope for the two load positions. This slope increases when the entrance length is increased.

3. The radial nonuniformities are of the same order of magnitude for the two positions (Fig. 9).

Conclusions of the experimental study.—The experimental study has allowed for identification of the typical features of silicon nitride deposition from LPCVD. On the one hand, axial variations are low,

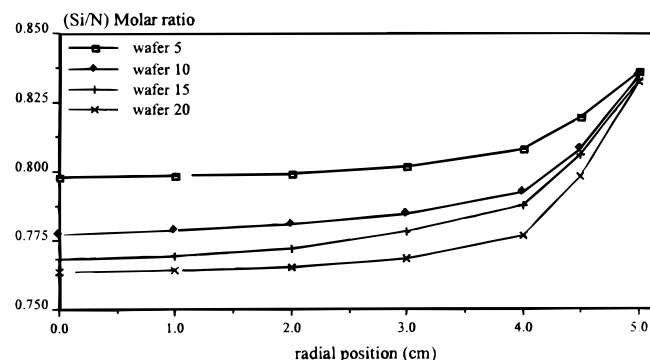


Figure 7. Radial evolution of silicon nitride composition at a temperature of 750°C for different wafer positions.

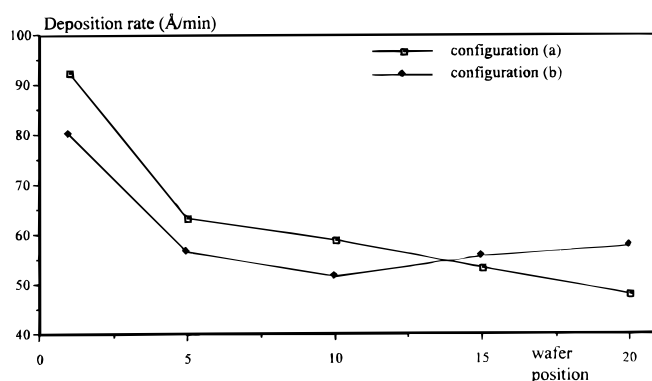


Figure 8. Longitudinal evolution of deposition rate for two load configurations.

which suggests that the composition of reactive species remains practically constant along the reactor. On the other hand, marked radial variations have been noted, which clearly involves the contribution of one (or several) reactive species sticking on the surface at the wafer periphery before they diffuse toward the center. To identify these species, a study on the gaseous phase chemical mechanism was achieved and is presented in what follows.

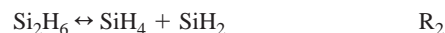
Development of a Gas Phase Mechanism

In this part, a complete gas phase mechanism obtained from a detailed literature analysis is first proposed. Then, a thorough QRRK analysis¹⁰ has compensated for the lack of kinetic information in the gas phase and a reduced reaction set reproducing the essential features of the full mechanism is presented.

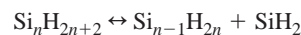
Gas phase chemistry of a silane-ammonia mixture.—*Silane pyrolysis.*—The mechanism of the thermal decomposition of silane is of considerable interest.¹¹⁻¹⁵ The primary decomposition in silane pyrolysis is the elimination of molecular hydrogen to form silylene according to



This reaction is then followed by



and, more generally



(The symbol \leftrightarrow represents forward and backward directions of the reaction).

As the concentration of reaction products R1 increases when n increases, the common assumption is not to consider higher order silanes than disilane. This hypothesis is still adopted in this study.^{6,7,9}

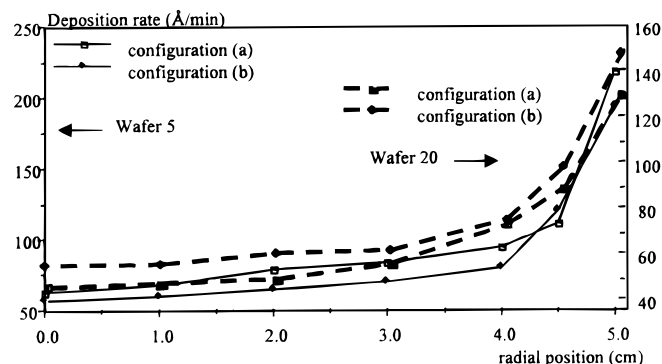


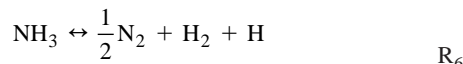
Figure 9. Radial evolution of deposition rate of wafers 5 and 20 for two load positions.

As the following reaction plays a major role in silicon nitride deposition by PECVD³



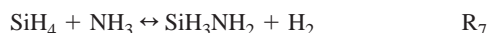
it has first been included in the gas phase mechanism. This has not been the case in our previous works on LPCVD silicon deposition from silane.

Ammonia pyrolysis.—Due to the electronegative character of nitrogen atom, ammonia pyrolysis seems difficult under LPCVD conditions. This is why only the first reaction of the following set was finally taken into account¹⁶

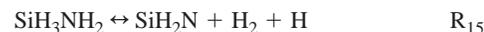
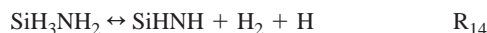
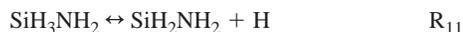
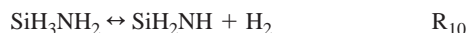
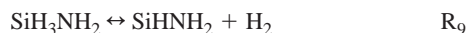


The high activation energies for reactions R4 and R5 (respectively, 122.1 and 200.7 kcal/mol) make pathways R4 and R5 relatively unimportant. They have thus been neglected in the final scheme.

Interaction between ammonia and silicon hydrides.—Two kinds of interactions can take place,¹⁷ according to the following reactions



SiH₃NH₂ pyrolysis.—This pyrolysis can lead to a large range of products, *i.e.*, SiH₂NH, SiH₂NH₂, SiH₃N, SiH₂NH, and SiHN¹⁸ according to the following reactions (R9 to R15)



According to Ref. 18, only reactions R9 to R12 have to be considered (the activation energies of reactions R13 to R15 are too high for the reactions to take place).

Reactions: molecule-radical and radical-radical.—For this set of reactions, a very complex mechanism is proposed in Ref. 18, where reactions R16 to R26 represent only a fraction. Particularly, the production of aminosilanes of order greater than one is neglected (both as regarded with Si and N). Their contribution is discussed in the analysis of QRRK results

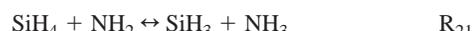
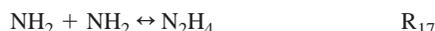
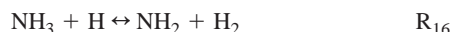


Table IV. Reaction mechanism.

| Reactions | Number |
|---|-----------------|
| $\text{SiH}_4 \leftrightarrow \text{SiH}_2 + \text{H}_2$ | R ₁ |
| $\text{Si}_2\text{H}_6 \leftrightarrow \text{SiH}_4 + \text{SiH}_2$ | R ₂ |
| $\text{SiH}_4 \leftrightarrow \text{SiH}_3 + \text{H}$ | R ₃ |
| $\text{NH}_3 \leftrightarrow \text{NH}_2 + \text{H}$ | R ₄ |
| $\text{SiH}_4 + \text{NH}_3 \leftrightarrow \text{SiH}_3\text{NH}_2 + \text{H}_2$ | R ₇ |
| $\text{SiH}_2 + \text{NH}_3 \leftrightarrow \text{SiH}_3\text{NH}_2$ | R ₈ |
| $\text{SiH}_3\text{NH}_2 \leftrightarrow \text{SiH}_2\text{NH} + \text{H}_2$ | R ₉ |
| $\text{SiH}_3\text{NH}_2 \leftrightarrow \text{SiH}_2\text{NH}_2 + \text{H}_2$ | R ₁₀ |
| $\text{SiH}_3\text{NH}_2 \leftrightarrow \text{SiH}_2\text{NH}_2 + \text{H}$ | R ₁₁ |
| $\text{SiH}_3\text{NH}_2 \leftrightarrow \text{SiH}_3 + \text{NH}_2$ | R ₁₂ |
| $\text{NH}_3 + \text{H} \leftrightarrow \text{NH}_2 + \text{H}_2$ | R ₁₆ |
| $\text{NH}_2 + \text{NH}_2 \leftrightarrow \text{N}_2\text{H}_4$ | R ₁₇ |
| $\text{NH}_3 + \text{NH}_2 \leftrightarrow \text{N}_2\text{H}_4 + \text{H}$ | R ₁₈ |
| $\text{SiH}_4 + \text{NH}_2 \leftrightarrow \text{SiH}_3\text{NH}_2 + \text{H}$ | R ₁₉ |
| $\text{SiH}_3 + \text{NH}_3 \leftrightarrow \text{SiH}_3\text{NH}_2 + \text{H}$ | R ₂₀ |
| $\text{SiH}_4 + \text{NH}_2 \leftrightarrow \text{SiH}_3 + \text{NH}_3$ | R ₂₁ |
| $\text{SiH}_4 + \text{H} \leftrightarrow \text{SiH}_3 + \text{H}_2$ | R ₂₂ |
| $\text{SiH}_4 + \text{SiH}_3 \leftrightarrow \text{Si}_2\text{H}_6 + \text{H}$ | R ₂₃ |
| $\text{SiH}_2 + \text{NH}_2 \leftrightarrow \text{SiH}_2\text{NH}_2$ | R ₂₄ |
| $\text{SiH}_2\text{NH}_2 + \text{H} \leftrightarrow \text{SiH}_2\text{NH}_2$ | R ₂₅ |
| $\text{SiH}_2\text{NH} + \text{H} \leftrightarrow \text{SiH}_2\text{NH}_2$ | R ₂₆ |

Gas phase mechanism.—With all these elements in mind, the studied gas phase mechanism is presented in Table IV.

Determination of the Absolute Rate Constants of the Reactions of the Proposed Mechanism

Kinetic modeling with a QRRK model.—The determination of the absolute rate constants for all the reactions presented in Table IV is an essential key of our approach. It was found by previous researchers^{11,19} that the monomolecular reactions were in their fall-off regions in LPCVD conditions: the rate constants are not only dependent on temperature but also on pressure. Following the guide lines of a previous study carried out for the determination of kinetic constants of pure SiH₄ and of an SiH₄-N₂O mixture under equivalent LPCVD conditions, computational techniques based on QRRK theory²⁰ were used to determine kinetic constants of the reactions proposed in Table IV. The input parameters for the calculation, presented in Tables V to VII are Lennard-Jones parameters,²¹ enthalpy and entropy of the reactions, activation energy, *E_∞*, and preexponential constant, *A_∞*, in standard conditions, equilibrium constants, number of harmonic oscillators, vibrational frequencies, and collision energy. Note that the unknown Lennard-Jones potential parameters (*σ* and *ε/k*) were calculated by linear interpolation with reference to analog species, as sug-

Table V. Molar weight and Lennard-Jones parameters of the different chemical species.

| Chemical species | Molar weight (g/mol) | <i>σ</i> : collision diameter (Å) | <i>ε/k</i> (°K ⁻¹) | References |
|----------------------------------|----------------------|-----------------------------------|--------------------------------|------------|
| SiH ₄ | 32.12 | 4.084 | 207.6 | 21 |
| SiH ₃ | 31.11 | 3.943 | 170.3 | 20 |
| SiH ₂ | 30.10 | 3.803 | 133.1 | 21 |
| Si ₂ H ₆ | 62.22 | 4.828 | 301.3 | 21 |
| H ₂ | 2.016 | 2.827 | 59.7 | 21 |
| H | 1.008 | 2.270 | 37.0 | 3 |
| SiH ₃ NH ₂ | 47.17 | 4.560 | 339.0 | 3 |
| SiH ₂ NH ₂ | 46.12 | 4.447 | 345.3 | calculated |
| SiH ₂ NH | 45.11 | 4.344 | 351.5 | calculated |
| NH ₃ | 17.03 | 2.9 | 558.3 | 21 |
| NH ₂ | 16.02 | 2.7 | 357.9 | calculated |
| N ₂ H ₄ | 32.04 | 4.28 | 475 | 3 |

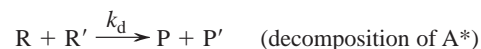
Table VI. Enthalpy and entropy of formation of the different chemical species.

| Chemical species | Enthalpy of formation (kcal/mol) | Entropy of formation (cal/mol K) |
|----------------------------------|----------------------------------|----------------------------------|
| SiH ₄ | 8.2 | 48.8 |
| SiH ₃ | 47.8 | 51.7 |
| SiH ₂ | 58.0 | 49.4 |
| Si ₂ H ₆ | 19.1 | 65.4 |
| H ₂ | 0.0 | 31.2 |
| H | 52.1 | 27.4 |
| NH ₃ | -11.0 | 45.9 |
| NH ₂ | 46.1 | 46.4 |
| N ₂ H ₄ | 12.1 | 28.9 |
| SiH ₃ NH ₂ | -11.5 | 65.7 |
| SiH ₂ NH ₂ | 28.0 | 65.8 |
| SiHNNH ₂ | 26.3 | 59.8 |
| SiH ₂ NH | 41.0 | 59.9 |

gested in Ref. 11. The preexponential constants were evaluated using approximations suggested by Troe.²² The equilibrium constants were computed by use of Benson's method. The collision energy, $\langle \Delta E_{\text{coll}} \rangle$, refers to the average energy exchanged between the present chemical species and the predominant species. According to the mixture nature (whether *i* is richer in silane or ammonia or conversely), the influence of one species or the other as a buffer gas may change QRRK computations. Since several simulations have shown that this parameter has only a weak influence on the final results, an equimolar mixture of silane and ammonia was finally chosen as the buffer gas. This result is the direct consequence of the same order of magnitude for collision energies for ammonia and silane^{3,20} ($\langle \Delta E_{\text{coll}} \rangle \text{NH}_3 = 2500 \text{ cal/mol}$, $\langle \Delta E_{\text{coll}} \rangle \text{SiH}_4 = 2100 \text{ cal/mol}$).

Note that two species R and R' [their formation kinetic constant is denoted $k_{1\infty} f(E)$] in a bimolecular reaction can react to give an activated complex (A*) which may be either stabilized by collision with inert molecules, either give reaction products or give back to reactant species. A schematic energetic diagram of a bimolecular reaction is proposed in Fig. 10. The stabilization rate constant of A* is also taken into account in the QRRK analysis. The application of quasi-stationary state principle to A* gives the expression of rate

constants of the following reactions, thus complicating the initial set of chemical reactions (R1 to R26)

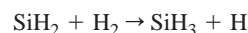


With this element in mind, a total of 35 kinetic reactions with 13 species was finally obtained. The same parameters as for unimolecular kinetic rate constants, applied to A* are input parameters of the model.

The computed kinetic rate constants for unimolecular and bimolecular reactions are presented in Tables VIII and IX. Arrhenius parameters for the rate constants in the forward direction are written in the form $k = AT^B \exp(-E/RT)$. The units of *A* depend on the reaction order, but are given in terms of moles, cubic meters, and seconds. *E* is in J/mole. Rate constants for the back reactions are calculated from the reaction thermochemistry.

Results of the kinetic study.—The main features of the kinetic study may be summarized as follows

(i) *Silane pyrolysis.*—The thermal decomposition of monosilane has been investigated by many authors¹¹⁻¹⁵ and recently in our laboratory. The computation results in this study are of the same order of magnitude as those previously reported, even if mathematical expressions may differ since LPCVD conditions and chemical environment are not the same.²⁰ Our study confirms that reaction



does not play a significant role in LPCVD conditions, even in presence of ammonia.

(ii) *Ammonia pyrolysis.*—Over the range of LPCVD operating conditions and for temperatures varying between 600 and 900°C, our kinetic study reveals that the formation of radicals from ammonia does not occur because of a too high energetic barrier. This situation corresponds to computed values for kinetic constants equal to zero (see Table IX). Consequently, the chemical system is controlled by species produced only by silane and not by ammonia pyrolysis.

(iii) *Production of SiH₃NH₂ aminosilane.*—Reactions R2 and R35 show that two kinds of interactions may initiate the production of

Table VII. Presentation of the complete data for the QRRK analysis.

| Chemical reaction | ΔH_r (kcal/mol) | ΔS_r (kcal/mol) | E_{ad} (kcal/mol) | E_{ai} (kcal/mol) | A_d | A_i | Number of harmonic oscillators | Vibrational frequency |
|--|-------------------------|-------------------------|----------------------------|----------------------------|-------------------------|--------------------------|--------------------------------|-----------------------|
| SiH ₂ + H ₂ → SiH ₄ | -49.2 | -31.8 | 7.7 | 56.9 | 1.991 × 10 ⁷ | 2.667 × 10 ¹⁶ | 10 | 1364 |
| SiH ₃ + H → SiH ₄ | -91.1 | -30.3 | 1.9 | 93 | 2.65 × 10 ⁸ | 1.669 × 10 ¹⁶ | 10 | 1364 |
| SiH ₄ + SiH ₂ → Si ₂ H ₆ | -46.5 | -32.8 | 5.29 | 51.79 | 1.185 × 10 ⁷ | 2.625 × 10 ¹⁷ | 19 | 927.7 |
| NH ₂ + H → NH ₃ | -106.9 | -27.9 | 0 | 107.5 | 1.926 × 10 ⁸ | 3.625 × 10 ¹⁷ | 7 | 2152 |
| SiH ₄ + NH ₃ → SiH ₃ NH ₂ + H ₂ | -8.7 | 2.2 | 55.4 | 64.1 | 1.416 × 10 ⁶ | 4.68 × 10 ⁸ | | |
| SiH ₂ + NH ₃ → SiH ₃ NH ₂ | -57.9 | -29.6 | 8.2 | 66.1 | 1.21 × 10 ⁶ | 5.326 × 10 ¹⁵ | 16 | 1155 |
| SiHNNH ₂ + H ₂ → SiH ₃ NH ₂ | -37.2 | -25.3 | 16.9 | 54.1 | 2.643 × 10 ⁶ | 1.344 × 10 ¹⁵ | 16 | 1155 |
| SiH ₂ NH + H ₂ → SiH ₃ NH ₂ | -51.9 | -25.4 | 24.1 | 76 | 2.643 × 10 ⁷ | 1.414 × 10 ¹⁵ | 16 | 1155 |
| SiH ₂ NH ₂ + H → SiH ₃ NH ₂ | -91 | 27.5 | 3.5 | 94.5 | 3.429 × 10 ⁸ | 5.278 × 10 ¹⁴ | 16 | 1155 |
| SiH ₃ + NH ₂ → SiH ₃ NH ₂ | -104.8 | -32.4 | 2.9 | 107.7 | 1.115 × 10 ⁸ | 1.366 × 10 ¹⁴ | 16 | 1155 |
| SiH ₂ + NH ₂ → SiH ₂ NH ₂ | -75.5 | -30 | 2.1 | 77.6 | 1.066 × 10 ⁸ | 5.77 × 10 ¹⁵ | 13 | 1222 |
| SiHNNH ₂ + H → SiH ₂ NH ₂ | -49.8 | -21.4 | 1.3 | 51.1 | 3.335 × 10 ⁸ | 2.38 × 10 ¹⁴ | 13 | 1222 |
| SiH ₂ NH + H → SiH ₂ NH ₂ | -64.5 | -21.5 | 1.6 | 66.1 | 3.335 × 10 ⁸ | 2.51 × 10 ¹⁴ | 13 | 1222 |
| NH ₃ + H → NH ₂ + H ₂ | 5 | 4.3 | 16.4 | 11.4 | 2.24 × 10 ⁷ | 2.57 × 10 ⁹ | | |
| NH ₂ + NH ₂ → N ₂ H ₄ | -79.5 | -63.8 | 0.5 | 80 | 1.013 × 10 ⁸ | 1.405 × 10 ²³ | 13 | 2023 |
| NH ₃ + NH ₂ → N ₂ H ₄ + H | 29.1 | -36 | 59.2 | 30.1 | 1.18 × 10 ⁷ | 8.715 × 10 ¹⁷ | | |
| NH ₂ + SiH ₄ → SiH ₃ NH ₂ + H | -13.7 | -2.1 | 14.4 | 28.1 | 1.25 × 10 ⁷ | 3.595 × 10 ¹⁰ | | |
| NH ₂ + SiH ₄ → SiH ₃ + NH ₃ | -17.5 | 2.4 | 9.7 | 27.2 | 1.25 × 10 ⁷ | 3.73 × 10 ⁹ | | |
| NH ₃ + SiH ₃ → SiH ₃ NH ₃ + H | 3.8 | -4.5 | 27.2 | 23.4 | 1.31 × 10 ⁷ | 1.26 × 10 ¹¹ | | |
| SiH ₄ + H → SiH ₃ + H ₂ | -12.5 | 6.7 | 8.2 | 20.7 | 2.852 × 10 ⁷ | 9.795 × 10 ⁸ | | |
| SiH ₂ NH ₂ + H → SiH ₃ NH ₂ | 15.2 | -7.7 | 30.3 | 15.1 | 1.266 × 10 ⁷ | 6.1 × 10 ¹¹ | | |

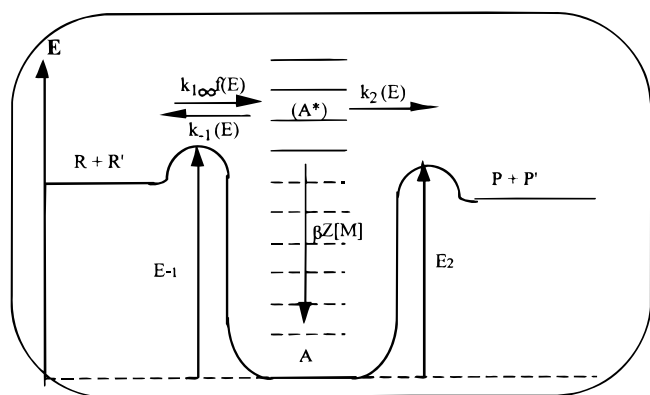
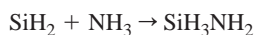


Figure 10. Energetic diagram of a bimolecular reaction.

SiH_3NH_2 . The QRRK computation finally reports that reaction R35 is negligible toward reaction R2 (the direct constant ratio is about 2×10^{-11}).

(iv) *Competitive reactions.*—The key component of the chemical system, *i.e.*, silylene, can enter into two kinds of reactions, either



or



A comparison of the energetic level of the produced species shows that the aminosilane molecule is far more stable than disilane, since there is a discrepancy of 30.6 kcal/mol in their activation energy. This element suggests silylene rather reacts with ammonia than with silane, which is confirmed by a comparative analysis of the ratio between the direct and backward kinetic constants (it is equal to 2.5×10^6 for the first reaction and to 2.6×10^2 for the second one).

Development of a simplified mechanism.—The accounting of all these gas phase reactions in a more complex model representing the physicochemical phenomena occurring in an LPCVD reactor would be practically irrelevant, because of excessive central processing unit time requirements. The next step of our approach is to simplify the reaction scheme to be then included in an LPCVD deposition model.

First analysis of the chemical system.—Using the whole mechanism, the time evolution of all the species concentrations which could be observed in a hypothetical gas volume, uniform in its properties and without any contact with solid surfaces, starting from the mixture of silane and ammonia was computed using numerical integration based on Gear's method.⁹ Typical results obtained are presented in Fig. 11 for a temperature of 650°C, a pressure set at 0.4 Torr, and a silane/ammonia ratio equal to 0.4/0.6.

The contribution of high-order aminosilane such as $\text{SiH}_2(\text{NH}_2)_2$, $\text{SiH}(\text{NH}_2)_3$, $\text{Si}(\text{NH}_2)_4$, and radical species produced from these molecules was previously mentioned. This study confirms that neither of these species is significant enough to influence the final chemical mechanism; a distinction must now be made between radical and stable species.

On the one hand, disilane and hydrazine, which are stable molecules, have very low concentrations relative to the concentrations of the other stable species, *i.e.*, silane and hydrogen. A series of simulation runs was performed in which secondary reactions of these species were neglected. The results obtained showed that the evolution of the remaining species of the system is not affected by this modification.

On the other hand, even in very low concentrations, silylamine radicals, *i.e.*, SiHNH_2 , SiH_2NH , and SiH_2NH_2 (respectively, 2.8×10^{-4} , 1.3×10^{-8} , and 2.1×10^{-8}) may have a nonnegligible impact on the whole mechanism. Due to the similar atomic structure of these species, it could be assumed that their contribution to deposition rate was directly dependent on the molar fraction of the species.

Because the SiHNH_2 molar fraction is approximately 10^4 times greater than the other ones, its contribution will mask the effect of the other species.

A similar analysis has been applied to the cases of SiH_2 and SiH_3 . It has led to the elimination of SiH_3 in the chemical mechanism (see Fig. 11). The hydrogen atom does not play a significant role since as soon as it adsorbs on a surface, it recombines to give molecular hydrogen. The concentration of NH_2 radical is too low to compete seriously with NH_3 (its molar fraction is about 10^{-10}) during deposition and can thus be neglected. This approach has been repeated for a wide range of temperatures, pressures and silane/ammonia ratios. In all cases, the same species have been candidates for elimination and have been definitely removed from the complete scheme.

Finally, a reduced reaction set (see Table X) which reproduces the essential features of the full mechanism and involves only six species including two silylamine intermediates, *i.e.*, SiH_3NH_2 (stable) and SiHNH_2 (reactive) has been adopted.

Influence of operating conditions.—*Influence of temperature.*—An increase in temperature has a noticeable effect on molar fractions of the different species. At a temperature of 750°C, the molar fractions of SiH_3NH_2 , SiHNH_2 , and H_2 are multiplied to 15 times that corresponding to 650°C, whereas the molar fraction of SiH_2 is increased to 25 times that (Fig. 12). It can therefore be suggested that an increase in temperature will involve an increase in deposition rate as well as in the nonuniformity at the wafer periphery, concerning both thickness and silicon amount.

Table VIII. Kinetic constants for unimolecular reactions; pressure is in Pa, temperature in K and $R = 8.314 \text{ J mol}^{-1} \text{ K}^{-1}$.

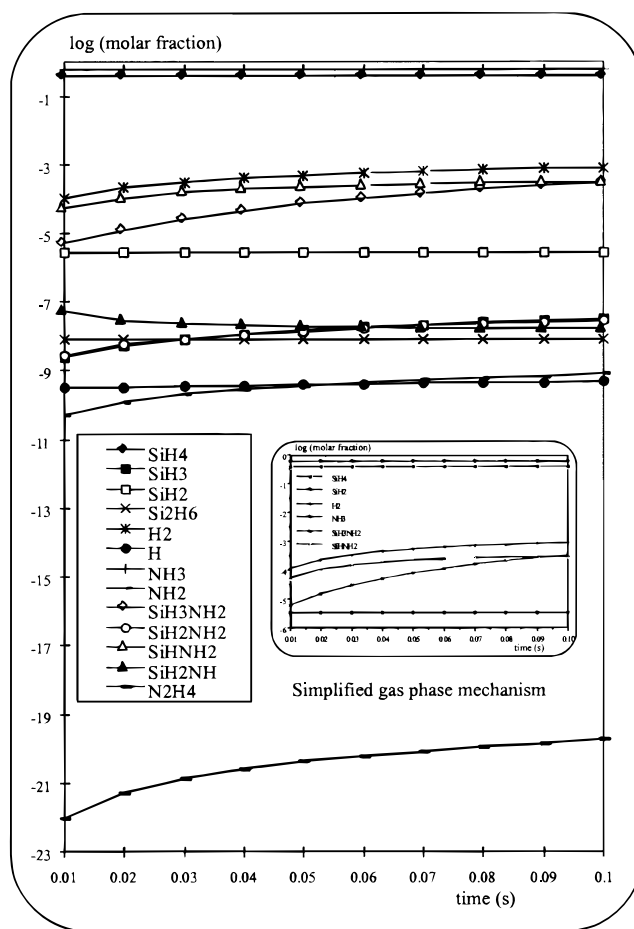
| Chemical reactions | Kinetic constants for unimolecular reactions ($\text{m}^3 \text{ mol}^{-1} \text{ s}^{-1}$ or s^{-1}) according to the reaction order |
|--|--|
| $\text{SiH}\text{NH}_2 + \text{H}_2 \rightarrow \text{SiH}_3\text{NH}_2$ | $k_1 = 1.585 \times 10^{-2} P^{0.87} \exp(121.4 \times 10^3/RT)$ $k_{-1} = 1.258 \times 10^9 P^{0.97} \exp(-178.09 \times 10^3/RT)$ |
| $\text{SiH}_2 + \text{NH}_3 \rightarrow \text{SiH}_3\text{NH}_2$ | $k_2 = 17.4 \times 10^{-2} P^{1.0} \exp(64.53 \times 10^3/RT)$ $k_{-2} = 3.23 \times 10^8 P^{1.0} \exp(-227.51 \times 10^3/RT)$ |
| $\text{SiH}_2\text{NH} + \text{H}_2 \rightarrow \text{SiH}_3\text{NH}_2$ | $k_3 = 0.145 P^{1.0} \exp(133.98 \times 10^3/RT)$ $k_{-3} = 0.0$ |
| $\text{SiH}_2\text{NH}_2 + \text{H} \rightarrow \text{SiH}_3\text{NH}_2$ | $k_4 = 0.5 P^{1.0} \exp(42.14 \times 10^3/RT)$ $k_{-4} = 0.0$ |
| $\text{SiH}_3 + \text{NH}_2 \rightarrow \text{SiH}_3\text{NH}_2$ | $k_5 = 0.074 P^{1.0} \exp(37.06 \times 10^3/RT)$ $k_{-5} = 0.0$ |
| $\text{SiH}\text{NH}_2 + \text{H} \rightarrow \text{SiH}_2\text{NH}_2$ | $k_6 = 269.2 P^{0.96} \exp(49.01 \times 10^3/RT)$ $k_{-6} = 2.08 \times 10^8 P^{1.0} \exp(-172.52 \times 10^3/RT)$ |
| $\text{SiH}_2\text{NH} + \text{H} \rightarrow \text{SiH}_2\text{NH}_2$ | $k_7 = 11.97 P^{1.0} \exp(38.25 \times 10^3/RT)$ $k_{-7} = 1.70 \times 10^7 P^{1.0} \exp(-240.16 \times 10^3/RT)$ |
| $\text{SiH}_2 + \text{NH}_2 \rightarrow \text{SiH}_2\text{NH}_2$ | $k_8 = 1.07 P^{1.0} \exp(34.37 \times 10^3/RT)$ $k_{-8} = 0.0$ |
| $\text{SiH}_2 + \text{H}_2 \rightarrow \text{SiH}_4$ | $k_9 = 0.074 P^{1.0} \exp(66.27 \times 10^3/RT)$ $k_{-9} = 1.24 \times 10^8 P^{1.0} \exp(-205.65 \times 10^3/RT)$ |
| $\text{SiH}_3 + \text{H} \rightarrow \text{SiH}_4$ | $k_{10} = 1.04 \times 10^{-2} P^{1.0} \exp(38.25 \times 10^3/RT)$ $k_{-10} = 0.0$ |
| $\text{SiH}_2 + \text{SiH}_4 \rightarrow \text{Si}_2\text{H}_6$ | $k_{11} = 0.021 P^{0.95} \exp(95.85 \times 10^3/RT)$ $k_{-11} = 4.69 \times 10^8 P^{0.99} \exp(-143.60 \times 10^3/RT)$ |
| $\text{NH}_2 + \text{H} \rightarrow \text{NH}_3$ | $k_{12} = 10.08 P^{1.0} \exp(19.42 \times 10^3/RT)$ $k_{-12} = 0.0$ |
| $\text{NH}_2 + \text{NH}_2 \rightarrow \text{N}_2\text{H}_4$ | $k_{13} = 1.88 \times 10^{-6} P^{1.0} \exp(26.72 \times 10^3/RT)$ $k_{-13} = 0.0$ |

Table IX. Kinetic constants for bimolecular reactions.

| Chemical reactions | Kinetic constant for bimolecular reactions ($\text{m}^3 \text{mol}^{-1} \text{s}^{-1}$ or s^{-1}) |
|---|--|
| $\text{SiH}_2 + \text{NH}_3 \rightarrow \text{SiH}_2\text{NH}_2 + \text{H}_2$ | $k_{14} = 4.082 \times 10^4 \exp(34.97 \times 10^3/RT)$ |
| $\text{SiH}_2 + \text{NH}_3 \rightarrow \text{SiH}_2\text{NH} + \text{H}_2$ | $k_{-14} = 9.21 \times 10^1 \exp(16.18 \times 10^3/RT)$ |
| $\text{SiH}_2 + \text{NH}_3 \rightarrow \text{SiH}_2\text{NH}_2 + \text{H}$ | $k_{15} = 1.64 \times 10^6 \exp(-22.63 \times 10^3/RT)$ |
| $\text{SiH}_2 + \text{NH}_3 \rightarrow \text{SiH}_2\text{NH} + \text{H}$ | $k_{-15} = 1.4 \times 10^6 \exp(55.04 \times 10^3/RT)$ |
| $\text{SiH}_2 + \text{NH}_3 \rightarrow \text{SiH}_2\text{NH}_2 + \text{H}_2$ | $k_{16} = 5.63 \times 10^5 \exp(-77.49 \times 10^3/RT)$ |
| $\text{SiH}_2 + \text{NH}_3 \rightarrow \text{SiH}_2\text{NH} + \text{H}_2$ | $k_{-16} = 1.53 \times 10^8 \exp(7.19 \times 10^3/RT)$ |
| $\text{SiH}_2 + \text{NH}_3 \rightarrow \text{SiH}_2\text{NH}_2 + \text{H}$ | $k_{17} = 1.09 \times 10^5 \exp(-134.42 \times 10^3/RT)$ |
| $\text{SiH}_2 + \text{NH}_3 \rightarrow \text{SiH}_2\text{NH} + \text{H}$ | $k_{-17} = 5.16 \times 10^7 \exp(7.73 \times 10^3/RT)$ |
| $\text{SiH}_2 + \text{NH}_3 \rightarrow \text{SiH}_2\text{NH}_2 + \text{H}_2$ | $k_{18} = 2.19 \times 10^7 \exp(-24.75 \times 10^3/RT)$ |
| $\text{SiH}_2 + \text{NH}_3 \rightarrow \text{SiH}_2\text{NH} + \text{H}_2$ | $k_{-18} = 2.18 \times 10^6 \exp(43.11 \times 10^3/RT)$ |
| $\text{SiH}_2 + \text{NH}_3 \rightarrow \text{SiH}_2\text{NH}_2 + \text{H}$ | $k_{19} = 6.62 \times 10^6 \exp(-63.60 \times 10^3/RT)$ |
| $\text{SiH}_2 + \text{NH}_3 \rightarrow \text{SiH}_2\text{NH} + \text{H}$ | $k_{-19} = 2.36 \times 10^8 \exp(7.75 \times 10^3/RT)$ |
| $\text{SiH}_2 + \text{NH}_3 \rightarrow \text{SiH}_2\text{NH}_2 + \text{H}_2$ | $k_{20} = 3.57 \times 10^5 \exp(-138.5 \times 10^3/RT)$ |
| $\text{SiH}_2 + \text{NH}_3 \rightarrow \text{SiH}_2\text{NH} + \text{H}_2$ | $k_{-20} = 7.0 \times 10^7 \exp(13.73 \times 10^3/RT)$ |
| $\text{SiH}_2 + \text{NH}_3 \rightarrow \text{SiH}_2\text{NH}_2 + \text{H}$ | $k_{21} = 1.16 \times 10^7 \exp(-3.54 \times 10^3/RT)$ |
| $\text{SiH}_2 + \text{NH}_3 \rightarrow \text{SiH}_2\text{NH} + \text{H}$ | $k_{-21} = 8.71 \times 10^3 \exp(-35.1 \times 10^3/RT)$ |
| $\text{SiH}_2 + \text{NH}_3 \rightarrow \text{SiH}_2\text{NH}_2 + \text{H}_2$ | $k_{22} = 3.93 \times 10^6 \exp(0.8 \times 10^3/RT)$ |
| $\text{SiH}_2 + \text{NH}_3 \rightarrow \text{SiH}_2\text{NH} + \text{H}_2$ | $k_{-22} = 1.57 \times 10^5 \exp(-69.6 \times 10^3/RT)$ |
| $\text{SiH}_2 + \text{NH}_3 \rightarrow \text{SiH}_2\text{NH}_2 + \text{H}$ | $k_{23} = 2.20 \times 10^5 \exp(-17.45 \times 10^3/RT)$ |
| $\text{SiH}_2 + \text{NH}_3 \rightarrow \text{SiH}_2\text{NH} + \text{H}$ | $k_{-23} = 4.48 \times 10^8 \exp(-55.94 \times 10^3/RT)$ |
| $\text{SiH}_2 + \text{NH}_3 \rightarrow \text{SiH}_2\text{NH}_2 + \text{H}_2$ | $k_{24} = 4.48 \times 10^8 \exp(-55.94 \times 10^3/RT)$ |
| $\text{SiH}_2 + \text{NH}_3 \rightarrow \text{SiH}_2\text{NH} + \text{H}_2$ | $k_{-24} = 3.14 \times 10^8 \exp(7.11 \times 10^3/RT)$ |

Kinetic constant for unimolecular reactions ($\text{m}^3 \text{mol}^{-1} \text{s}^{-1}$ or s^{-1})

| Chemical reactions | Kinetic constant for unimolecular reactions ($\text{m}^3 \text{mol}^{-1} \text{s}^{-1}$ or s^{-1}) |
|---|---|
| $\text{SiH}_2\text{NH}_2 + \text{H} \rightarrow \text{SiH}_2 + \text{NH}_2$ | $k_{25} = 6.08 \times 10^9 \exp(-109.6 \times 10^3/RT)$ |
| $\text{SiH}_2\text{NH} + \text{H} \rightarrow \text{SiH}_2 + \text{NH}_2$ | $k_{26} = 8.99 \times 10^7 \exp(9.8 \times 10^3/RT)$ |
| $\text{SiH}_2 + \text{H}_2 \rightarrow \text{SiH}_3 + \text{H}$ | $k_{27} = 1.4 \times 10^7 \exp(-2.04 \times 10^3/RT)$ |
| $\text{SiH}_2 + \text{H} \rightarrow \text{SiH}_3 + \text{H}_2$ | $k_{28} = 2.68 \times 10^8 \exp(7.84 \times 10^3/RT)$ |
| $\text{SiH}_2 + \text{H} \rightarrow \text{SiH}_3 + \text{H}$ | $k_{29} = 2.85 \times 10^7 \exp(-34.28 \times 10^3/RT)$ |
| $\text{SiH}_2 + \text{H} \rightarrow \text{SiH}_3 + \text{H}_2$ | $k_{-29} = 9.79 \times 10^8 \exp(-86.53 \times 10^3/RT)$ |
| $\text{SiH}_2 + \text{H} \rightarrow \text{SiH}_3 + \text{H}$ | $k_{30} = 1.27 \times 10^7 \exp(-126.6 \times 10^3/RT)$ |
| $\text{SiH}_2 + \text{H} \rightarrow \text{SiH}_3 + \text{H}_2$ | $k_{31} = 6.10 \times 10^{11} \exp(-63.12 \times 10^3/RT)$ |
| $\text{NH}_3 + \text{H} \rightarrow \text{NH}_2 + \text{H}_2$ | $k_{32} = 2.24 \times 10^7 \exp(-68.55 \times 10^3/RT)$ |
| $\text{NH}_3 + \text{H} \rightarrow \text{NH}_2 + \text{H}$ | $k_{33} = 2.59 \times 10^9 \exp(-47.65 \times 10^3/RT)$ |
| $\text{NH}_3 + \text{H} \rightarrow \text{NH}_2 + \text{H}_2$ | $k_{34} = 1.18 \times 10^7 \exp(-247.4 \times 10^3/RT)$ |
| $\text{NH}_2 + \text{H} \rightarrow \text{NH}_3 + \text{H}$ | $k_{35} = 8.72 \times 10^{17} \exp(-125.8 \times 10^3/RT)$ |
| $\text{NH}_2 + \text{H} \rightarrow \text{NH}_3 + \text{H}_2$ | $k_{-35} = 1.25 \times 10^7 \exp(-60.19 \times 10^3/RT)$ |
| $\text{NH}_2 + \text{H} \rightarrow \text{NH}_3 + \text{H}_2$ | $k_{36} = 3.59 \times 10^{10} \exp(117.5 \times 10^3/RT)$ |
| $\text{NH}_2 + \text{H} \rightarrow \text{NH}_3 + \text{H}$ | $k_{37} = 1.25 \times 10^7 \exp(-40.55 \times 10^3/RT)$ |
| $\text{NH}_2 + \text{H} \rightarrow \text{NH}_3 + \text{H}_2$ | $k_{38} = 3.73 \times 10^9 \exp(-113.7 \times 10^3/RT)$ |
| $\text{NH}_2 + \text{H} \rightarrow \text{NH}_3 + \text{H}$ | $k_{39} = 1.31 \times 10^7 \exp(-113.7 \times 10^3/RT)$ |
| $\text{NH}_2 + \text{H} \rightarrow \text{NH}_3 + \text{H}_2$ | $k_{40} = 1.26 \times 10^{11} \exp(-97.8 \times 10^3/RT)$ |
| $\text{NH}_2 + \text{H} \rightarrow \text{NH}_3 + \text{H}$ | $k_{41} = 1.42 \times 10^6 \exp(-231.6 \times 10^3/RT)$ |
| $\text{NH}_2 + \text{H} \rightarrow \text{NH}_3 + \text{H}_2$ | $k_{42} = 4.68 \times 10^8 \exp(-267.9 \times 10^3/RT)$ |

Figure 11. Molar fraction profiles vs. time ($\text{NH}_3/\text{SiH}_4 = 0.6/0.4$; $T = 650^\circ\text{C}$; $P = 0.4$ Torr). Complete and simplified gas phase mechanisms.

Influence of pressure.—The influence of pressure has a weak effect on the system temporal evolution. As pressure increases, the molar fractions of SiH_2NH_2 and SiH_2 radicals decrease whereas the molar fraction of SiH_3NH_2 increases (Fig. 13). This suggests that the radical nonuniformities should decrease with increasing pressure. It will be clearly shown in the second part of this paper that these hetero-

Table X. Homogeneous gas phase mechanism adopted in this study.

| Chemical reaction | Kinetic constants (results of QRRK analysis) ($R = 8.314 \text{ J mol}^{-1} \text{ K}^{-1}$, P is in [Pa]) |
|---|--|
| $\text{SiH}_2 + \text{H}_2 \rightarrow \text{SiH}_4$ | $k_9 = 0.074 P^{1.0} \exp(66.27 \times 10^3/RT)$ $k_{-9} = 1.24 \times 10^8 P^{1.0} \exp(-205.65 \times 10^3/RT)$ |
| $\text{SiH}_2 + \text{NH}_3 \rightarrow \text{SiH}_3\text{NH}_2$ | $k_2 = 17.4 \times 10^{-2} P^{1.0} \exp(64.53 \times 10^3/RT)$ $k_{-2} = 3.23 \times 10^8 P^{1.0} \exp(-227.51 \times 10^3/RT)$ |
| $\text{SiH}_2\text{NH}_2 + \text{H}_2 \rightarrow \text{SiH}_3\text{NH}_2$ | $k_1 = 1.585 \times 10^{-2} P^{0.87} \exp(121.4 \times 10^3/RT)$ $k_{-1} = 1.258 \times 10^9 P^{0.97} \exp(-178.09 \times 10^3/RT)$ |
| $\text{SiH}_2 + \text{NH}_3 \rightarrow \text{SiH}_2\text{NH}_2 + \text{H}_2$ | $k_{14} = 4.082 \times 10^4 \exp(34.97 \times 10^3/RT)$ $k_{-14} = 9.21 \times 10^1 \exp(16.18 \times 10^3/RT)$ |

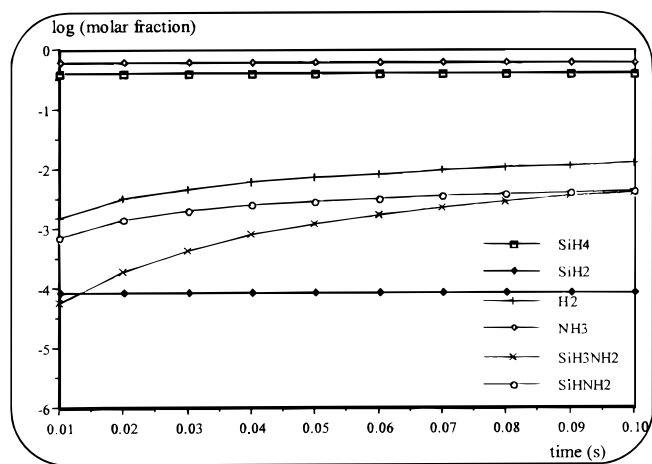


Figure 12. Molar fraction profiles vs. time ($\text{NH}_3/\text{SiH}_4 = 0.6/0.4$; $T = 750^\circ\text{C}$; $P = 0.4$ Torr). Simplified gas phase mechanisms.

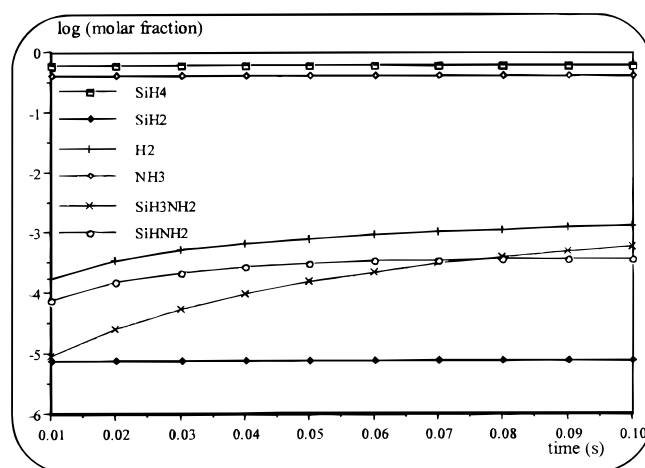


Figure 14. Molar fraction profiles vs. time ($\text{NH}_3/\text{SiH}_4 = 0.4/0.6$; $T = 650^\circ\text{C}$; $P = 0.4$ Torr). Simplified gas phase mechanisms.

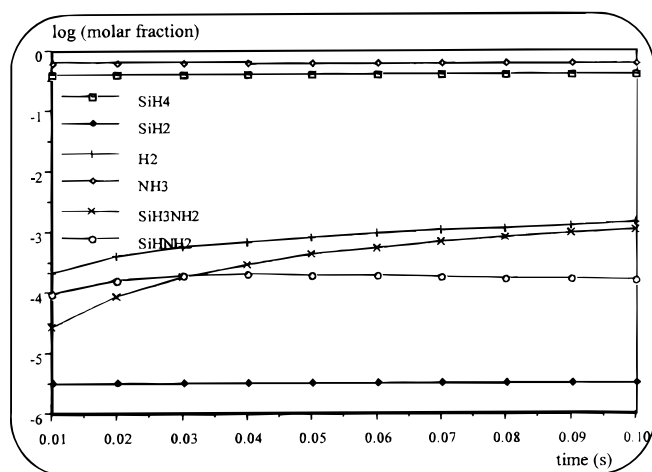


Figure 13. Molar fraction profiles vs. time ($\text{NH}_3/\text{SiH}_4 = 0.6/0.4$; $T = 650^\circ\text{C}$; $P = 0.8$ Torr). Simplified gas phase mechanisms.

geneties result from the contribution of SiHNNH_2 and SiH_2 radicals to deposition rate.

Influence of SiH_4/NH_3 ratio.—As silane is the only source for silylene, it can be expected that use of a rich silane feed would multiply the molar fraction of SiH_2 by a factor 3 and slightly increase the molar fraction of SiH_3NH_2 as well as of SiHNNH_2 (Fig. 14). These elements will be confirmed in the next modeling step of LPCVD deposition, including surface kinetics, since they explain the bull's eye effect experimentally observed as well as variations on silicon and nitrogen amounts at the wafer edge.

Conclusion

A gaseous reaction model has been proposed for a silane-ammonia mixture under typical LPCVD conditions. A complete reaction scheme base is first studied. A thorough QRKK analysis, compensating for the lack of kinetic information in the gas phase, has allowed the identification of kinetic constants for uni- and bimolecular reactions. Its appropriateness is examined with one-dimensional nonsteady computations. Then, a combined analysis of these calculations and of the QRRK results show that the reaction model could be simplified, thus leading to a reduced reaction set reproducing the essential features of the full mechanism experimentally observed. It involves six species with two silylamine intermediates: SiH_3NH_2 and SiHNNH_2 . In Part II of this paper, this mechanism will be integrated in a more complex model, taking into account mass transfer in the gas phase toward the surfaces and surface reactions.

Ecole Nationale Supérieure D'Ingenieris de Qenie Chimique, Institut National Polytechnique assisted in meeting the publication costs of this article.

List of Symbols

| | |
|--|--|
| A | preexponential constant ($\text{m}^3 \text{mol}^{-1} \text{s}^{-1}$ or s^{-1}) |
| A_d | preexponential constant (forward direction) ($\text{m}^3 \text{mol}^{-1} \text{s}^{-1}$ or s^{-1}) |
| A_i | preexponential constant (backward direction) ($\text{m}^3 \text{mol}^{-1} \text{s}^{-1}$ or s^{-1}) |
| d_i | thickness of film i (Å) |
| E_a | activation energy (kcal mol^{-1}) |
| E_d | activation energy (forward direction) (kcal mol^{-1}) |
| E_i | activation energy (backward direction) (kcal mol^{-1}) |
| k_d | reaction kinetic constant (forward direction) ($\text{m}^3 \text{mol}^{-1} \text{s}^{-1}$ or s^{-1}) |
| k_i | reaction kinetic constant (backward direction) ($\text{m}^3 \text{mol}^{-1} \text{s}^{-1}$ or s^{-1}) |
| n | refractive index (—) |
| P | pressure (Pa) |
| R | gas law constant ($\text{J mol}^{-1} \text{K}^{-1}$) |
| x | Si/N molar ratio (—) |
| $\langle \Delta E_{\text{coll}} \rangle$ | Average energy exchanged by collision ($\text{J mol}^{-1} \text{K}^{-1}$) |
| ΔH_r | enthalpy of reaction (cal mol^{-1}) |
| ΔS_r | entropy of reaction ($\text{kcal mol}^{-1} \text{K}^{-1}$) |
| ϵ/κ | Lennard-Jones parameter (K) |
| σ | Lennard-Jones parameter (Å) |

References

- V. I. Belyi, L. L. Vasilyeva, A. S. Ginovker, V. A. Grtitsenko, S. M. Repinsky, S. P. Sinitza, T. P. Smirnova, and F. L. Edelman, *Silicon Nitride In Electronics*, Elsevier, Oxford (1988).
- K. L. Kouassi, Ph.D. Thesis, Université Paul Sabatier, Toulouse, France (1992).
- A. Dollet, J. P. Couderc, and B. Despax, *Plasma Sources Sci. Technol.*, **4**, 94 (1995).
- E. Dehan, P. Temple-Boyer, R. Henda, J. J. Pedroviejo, and E. Scheid, *Thin Solid Films*, **266**, 14 (1995).
- F. Roenigk and K. F. Jensen, *J. Electrochem. Soc.*, **134**, 1777 (1987).
- P. Duverneuil and J. P. Couderc, *J. Electrochem. Soc.*, **139**, 296 (1992).
- C. Azzaro, P. Duverneuil, and J. P. Couderc, *J. Electrochem. Soc.*, **139**, 305 (1992).
- C. Azzaro, P. Duverneuil, and J. P. Couderc, *Chem. Eng. J.*, **48**, 1915 (1993).
- A. Tounsi, E. Scheid, P. Duverneuil, and J. P. Couderc, *Can. J. Chem. Eng.*, **74**, 941 (1997).
- S. Benson, *Thermochemical Kinetics, Method for Estimation of Thermochemical Data and Rate Parameters*, 2nd ed., Wiley-Interscience, New York (1976).
- M. E. Coltrin, R. J. Kee, and J. A. Miller, *J. Electrochem. Soc.*, **133**, 1207 (1986).
- H. Purnell and R. Walsh, *Proc. R. Soc. London Ser. A*, **293**, 543 (1966).
- B. S. Meyerson and J. M. Jasinski, *J. Appl. Phys.*, **61**, 785 (1987).
- H. K. Moffat and K. F. Jensen, *J. Electrochem. Soc.*, **135**, 459 (1988).
- M. E. Coltrin, R. J. Kee, and G. H. Evans, *J. Electrochem. Soc.*, **136**, 819 (1989).
- A. Ishitani and S. Koseki, *Jpn. J. Appl. Phys.*, **29**, L2322 (1990).
- A. Tachibana, K. Yamaguchi, S. Kawauchi, Y. Kurosaki, and T. Yamabe, *J. Am. Chem. Soc.*, **114**, 7504 (1992).
- C. F. Melius and P. Ho, *J. Phys. Chem.*, **95**, 1410 (1991).
- F. Jensen, *Chem. Eng. Sci.*, **42**, 923, (1987).
- F. Fayolle, J. P. Couderc, and P. Duverneuil, *Adv. Mater.*, **2**, 265 (1996).
- R. Reid and K. T. Sherwood, *The Properties of Gases and Liquids*, McGraw-Hill, New York (1958).
- J. Troe, *Chem. Phys.*, **66**, 4758 (1977).